

Future PhD thesis of Sabine Lammers

Sabine Wedam Lammers

lammers@mail.desy.de

University of Wisconsin-Madison

Department of Physics

draftversion 1.0 : 16. September 2003

Abstract:

Contents

1	Introduction - Basics of Particle Physics	3
2	Theoretical Overview - Basics of Perturbative QCD	6
2.1	Hadron Spectroscopy	6
2.2	Confinement and Asymptotic Freedom	6
2.3	Deep Inelastic Scattering	6
2.3.1	Quark Parton Model	6
2.3.2	DIS Cross Section	6
2.3.3	DGLAP Evolution Equations and the Leading Log Approximation	6
2.3.4	BFKL Evolution	6
2.3.5	Double Leading-Log Approximation	6
2.3.6	CCFM - Unification of the DGLAP and BFKL Pictures	6
3	Experimental Setup	7
3.1	HERA Collider	7
3.2	ZEUS Experiment	7
3.2.1	Uranium-Scintillator Calorimeter	8
3.2.2	Central Tracking Detector	9
3.2.3	Trigger System	9
3.2.4	Luminosity Measurement	10
3.2.5	Preshower Detectors - Presampler and SRTD	10
4	Event Generators and Detector Simulation	11
4.1	Basics of a Monte Carlo Simulation	11
4.2	Parton Density Functions (PDF's)	11
4.3	Parton Evolution	11
4.3.1	Matrix-Element and Parton Shower Models (MEPS)	11
4.3.2	Color Dipole Model	11
4.3.3	CASCADE	11
4.4	Hadronisation Models	11
4.4.1	Lund String Model	11
4.4.2	Cluster Fragmentation	11
4.5	ISR/FSR Corrections	11
5	NLO QCD Predictions	12
5.1	DISENT Program	12
5.2	Theoretical Uncertainties	12
5.2.1	Renormalization Scale Dependence and Uncertainty	12
5.2.2	Uncertainty due to Parton Density Functions	12
5.3	Hadronisation Corrections	12
6	Jet Physics in DIS at HERA	13
6.1	Reconstruction of the Kinematic Variables	13
6.2	kT-cluster algorithm	13
6.3	Breit Frame	13
6.4	Energy Flow and Jets in the Forward Region	13

7	Event Selection	14
7.1	Triggering on DIS Events	14
7.1.1	GFLT	14
7.1.2	GSLT	15
7.1.3	TLT	15
7.2	Offline Event Reconstruction	16
7.2.1	Positron Reconstruction	16
7.2.2	Jet Reconstruction	17
7.2.3	Jet Energy Correction	17
7.2.4	Cuts to Reject Background	18
7.2.5	Phase Space Selection	18
8	Description of the analysis	20
8.1	Preliminary Studies of Jet Cross Sections in the Breit Frame . .	20
8.2	Inclusive Jet Cross Section	20
8.2.1	Control Plots	20
8.2.2	Resolutions	20
8.2.3	Purities, Efficiencies, Correction Factors	20
8.3	BGF Enhanced Phase Space Cross Section	20
8.3.1	Control Plots	20
8.3.2	Resolutions	20
8.3.3	Purities, Efficiencies, Correction Factors	20
8.4	Forward Jet Cross Section	20
8.4.1	Control Plots	20
8.4.2	Resolutions	20
8.4.3	Purities, Efficiencies, Correction Factors	20
9	Results	21
9.1	Measurement of the inclusive jet cross section	21
9.2	Measurement of the inclusive jet cross section in the BGF en- hanced phase space	21
9.3	Forward jet cross section	21
9.4	Systematic Uncertainties	21
10	Conclusion	22

1 Introduction - Basics of Particle Physics

The birth of particle physics began with very simple scattering experiments. For example, the Rutherford experiment of scattering alpha particles off of gold foil which led to the observation that the atom contains a very heavy, dense core later to be called the nucleus. Experiments like these were inspired by the first questions of particle physics: What are the building blocks of matter and how do those building blocks interact? One hundred years later, those are still the questions driving and directing particle physics research.

Since those times, the nucleon of the atom was discovered to contain protons and neutrons, and is enveloped by a cloud of electrons. The proton and neutron were discovered to be made up of particles called quarks which, along with leptons, of which the electron is one example, are the most fundamental, that is, structureless, building blocks of the atom currently known.

Much like the organization of the chemical elements into the Periodic Table, a classification of the fundamental particles observed in nature according to certain rules has been made that reflects the results of many scattering experiments performed even today. Much like Rutherford's method of analyzing the topology of the scattered electron to infer the existence of substructure in the nucleus of the atom, modern particle physics observes final state properties of particles in high-energy scattering experiments which lead to a natural classification system designed to describe the properties of the particles observed in nature. For example, the quarks and leptons can be classified according to their charge, spin and mass as shown in Table 1.

Flavor	Charge	Spin	Mass
up	$+\frac{2}{3}$	$+\frac{1}{2}$	3 MeV
down	$-\frac{1}{3}$	$+\frac{1}{2}$	6 MeV
charm	$+\frac{2}{3}$	$+\frac{1}{2}$	1.2 GeV
strange	$-\frac{1}{3}$	$+\frac{1}{2}$	120 MeV
top	$+\frac{2}{3}$	$+\frac{1}{2}$	174 GeV
bottom	$-\frac{1}{3}$	$+\frac{1}{2}$	4.25 GeV
e^\pm	± 1	$\frac{1}{2}$	0.51 MeV
μ	± 1	$\frac{1}{2}$	106 MeV
τ	± 1	$\frac{1}{2}$	1.78 GeV
ν_e	0	$\frac{1}{2}$	≤ 3 eV
ν_μ	0	$\frac{1}{2}$	≤ 0.19 MeV
ν_τ	0	$\frac{1}{2}$	≤ 18.2 MeV

Table 1: Classification of the fermions

Quarks are objects which are not observed isolated in nature. In fact, what we observe are compounds of quark systems, called mesons (2-quark systems) and baryons (3-quark systems). In addition to charge, spin and mass, these hadrons (multi-quark systems) display properties such as baryon number, strangeness and isospin, which allow us to further distinguish them from each other. Each combination of these properties, or quantum numbers, gives rise to a unique particle that can be observed in nature. As one can well imagine, the number of observed particles gets very large, and, even now, continues to grow.

Particle physics, in addition to classifying the matter particles, tries to understand how these particles interact. There are, up to now, four known forces in nature: gravity, the weak nuclear force, electromagnetism and the strong nuclear force. ~~The mediators of these forces have particle manifestations as well.~~ The electromagnetic force is mediated by photons. The two forces that exist only inside the nucleon of an atom, the weak and strong nuclear forces, are governed by the W and Z particles (weak) and the gluon (strong). These particles, although they can be described by the same properties (i.e. mass, spin, charge, etc.) as the quarks and leptons, obey very different physical laws. As a result, particle physics categorizes all the fundamental particles into two groups: fermions, which describe the behavior of quarks and leptons, and bosons, which describe the behavior of the force mediators.

The Standard Model of particle physics is ~~the state-of-the-art~~ understanding of both the classification schemes of the fundamental particles, and the way these particles behave. It is based on the principles of quantum field theory, and has successfully described ~~all~~ experimental data which has tested the weak and strong nuclear forces.

The goal of this thesis is to make a stringent test of the theory of the strong nuclear force, Quantum Chromodynamics (QCD). In particular, to test whether the currently accepted understanding of how quarks and gluons interact with each other inside the proton is valid ~~to the deepest kinematical magnification, and the smallest momentum~~ of the parton (quark or gluon) inside the proton. ~~Access~~ to these energies is given by deep inelastic electron-proton scattering (DIS), in which a photon is emitted from the incoming electron which breaks the proton apart in the collision. The particles emitted from the collision undergo a process of showering and clustering before depositing their energy in the detector. By measuring the energy and position of the final particles that enter the detector, we can extrapolate back to the initial particles that came out of the collision and ~~do~~ a statistical analysis of the final state topologies in order to test the predictive power of QCD.

This measurement is concerned with a certain class of DIS events in which a highly collimated stream of final-state particles, called a jet, is located in the forward region (direction of the incoming proton) of the detector. The data used for this analysis were collected by the ZEUS experiment during the 1996 and 1997 running periods. Events in which the parton participating in the collision has low fractional momentum (of the proton) and which contain a forward jet may not be well described by the most conventional QCD prescription, the one where the interaction of the partons in the proton are given by the DGLAP equation. ~~We~~ have attempted in this analysis to uncover a kinematic region in which DGLAP evolution begins to break down, and where a possible transition to BFKL dynamics (another description of the interaction between quarks and gluons) may begin. Such a discovery would be a major success for QCD, because it would show that the theoretical approach to modeling how the partons behave is valid in a completely different kinematical regime.

Three measurements of the forward jet cross section are described in this thesis, where each gets consecutively more focused on the region where BFKL dynamics are expected to dominate. The data are compared to the best QCD calculations currently available, in which the strong coupling constant is calculated to second order. The parton evolution for this calculation is given by DGLAP, so a deviation between data and the theoretical prediction could indi-

cate the onset of BFKL dynamics. The theoretical background and challenges are discussed in more detail in Chapter 2. A detailed description of the accelerator, detector, and data acquisition are found in Chapter 3. Chapters 4 and 5 describe the programs used for the theoretical calculations, unfolding of the cross section, and various corrections that need to be applied. An overview of the issues relevant to doing a jet measurement is given in Chapter 6. Chapters 8 and 9 hold the description of the unfolding of the cross section for all three measurements as well as the final cross sections. Chapter 10 will summarize the conclusions drawn from the measurements.

2 Theoretical Overview - Basics of Perturbative QCD

2.1 Hadron Spectroscopy

2.2 Confinement and Asymptotic Freedom

2.3 Deep Inelastic Scattering

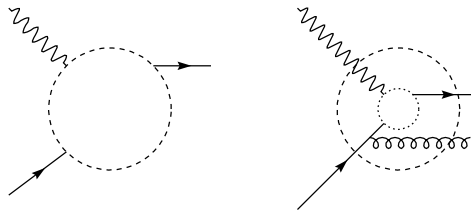


Figure 1:

2.3.1 Quark Parton Model

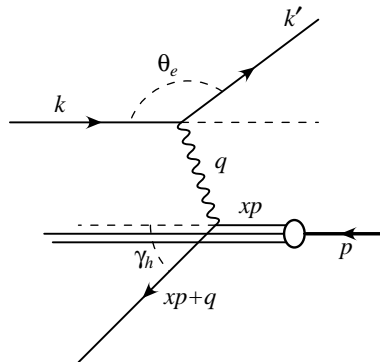


Figure 2:

2.3.2 DIS Cross Section

2.3.3 DGLAP Evolution Equations and the Leading Log Approximation

2.3.4 BFKL Evolution

2.3.5 Double Leading-Log Approximation

2.3.6 CCFM - Unification of the DGLAP and BFKL Pictures

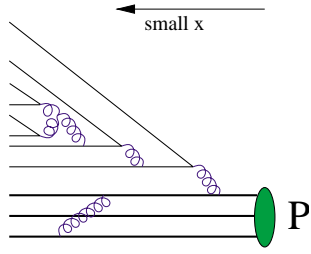


Figure 3:

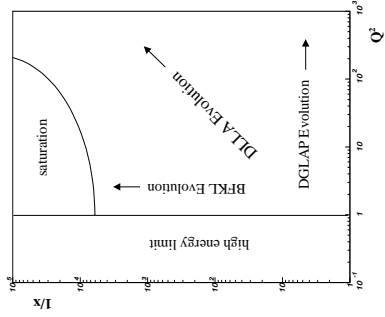


Figure 4:

3 Experimental Setup

3.1 HERA Collider

3.2 ZEUS Experiment

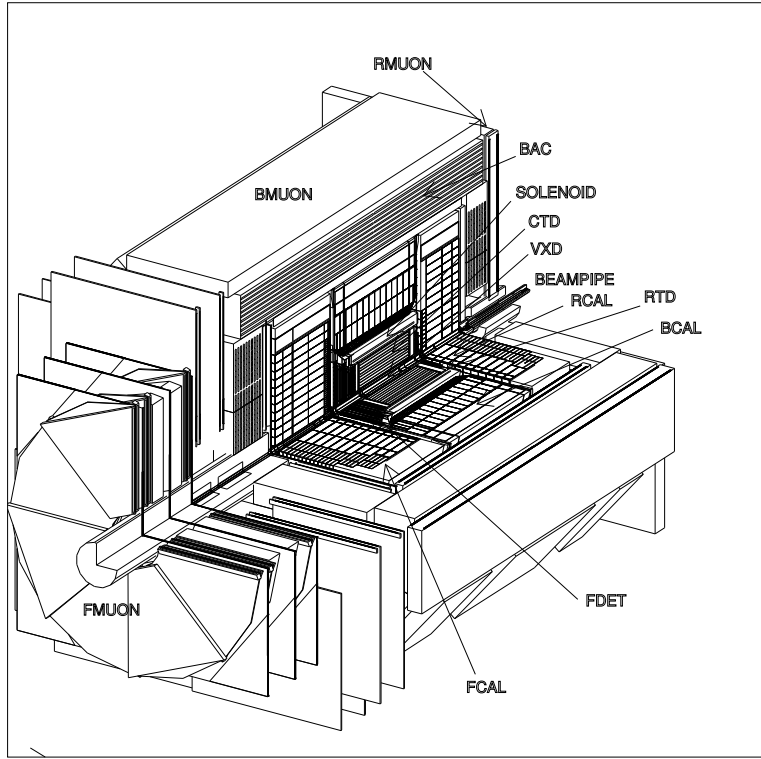


Figure 5:

3.2.1 Uranium-Scintillator Calorimeter

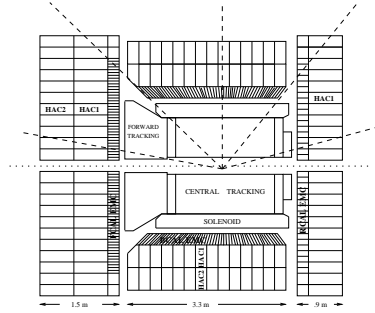


Figure 6:

3.2.2 Central Tracking Detector

3.2.3 Trigger System

Because of the 96 ns. crossing rate of the HERA accelerator, it is impossible to trigger on every event that occurs. In order to handle the speed at which the events are processed through the ZEUS data acquisition system, a three-tiered trigger has been built. At the first level,

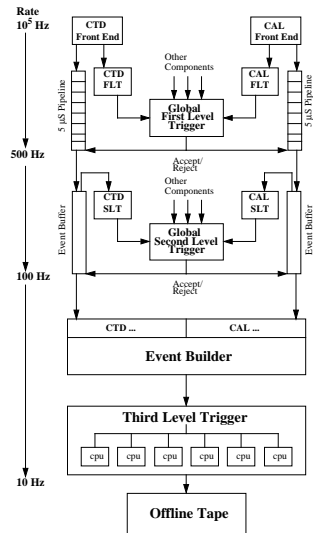


Figure 7:

3.2.4 Luminosity Measurement

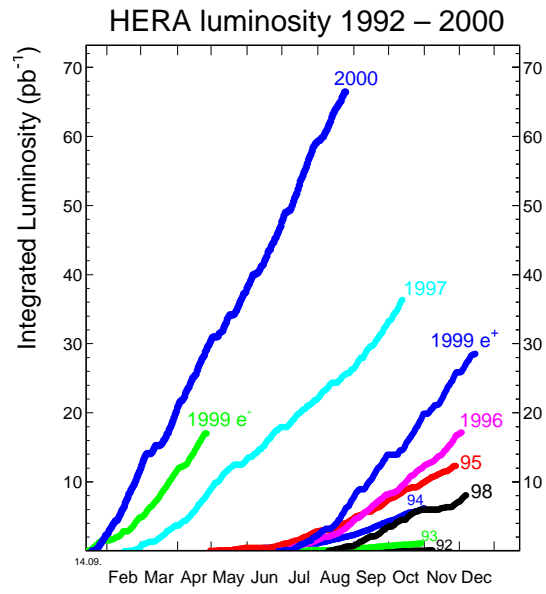


Figure 8:

3.2.5 Preshower Detectors - Presampler and SRTD

4 Event Generators and Detector Simulation

4.1 Basics of a Monte Carlo Simulation

4.2 Parton Density Functions (PDF's)

4.3 Parton Evolution

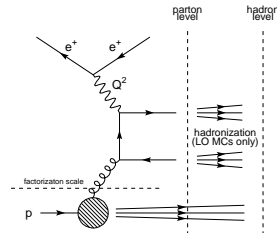


Figure 9:

4.3.1 Matrix-Element and Parton Shower Models (MEPS)

4.3.2 Color Dipole Model

4.3.3 CASCADE

4.4 Hadronisation Models

4.4.1 Lund String Model

4.4.2 Cluster Fragmentation

4.5 ISR/FSR Corrections

5 NLO QCD Predictions

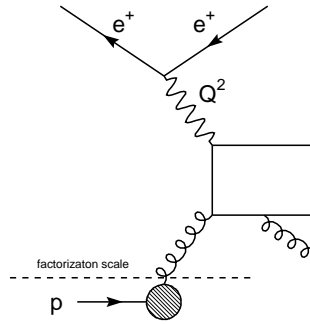


Figure 10:

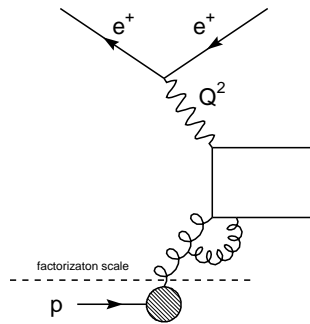


Figure 11:

5.1 DISENT Program

5.2 Theoretical Uncertainties

5.2.1 Renormalization Scale Dependence and Uncertainty

5.2.2 Uncertainty due to Parton Density Functions

5.3 Hadronisation Corrections

6 Jet Physics in DIS at HERA

6.1 Reconstruction of the Kinematic Variables

6.2 kT-cluster algorithm

6.3 Breit Frame

6.4 Energy Flow and Jets in the Forward Region

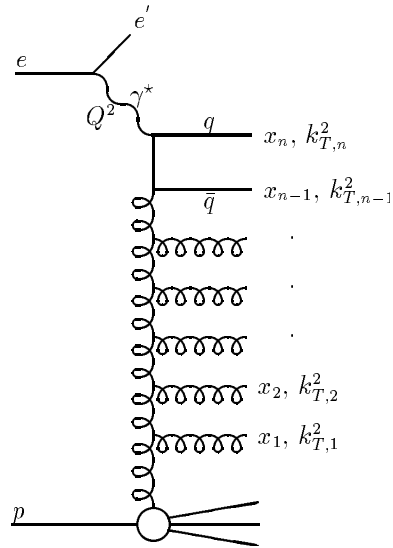


Figure 12:

7 Event Selection

Selecting the events that will be used for the measurements described in this thesis is a ~~many~~ step process. Neutral current DIS events must be triggered, various corrections applied to the raw data in order to ensure the measured energies and tracks are well reconstructed, cuts need to be applied to reject background, and the selection of the kinematic region pertinent to the analysis must be chosen. This analysis of forward jets is done with three separate measurements in three different phase space region. The first measurement is most inclusive and the basic trigger and background rejection requirements are developed for that analysis. Modifications to the kinematic region selected is made for the second and third measurement, as detailed in Sec. 7.2.5.

7.1 Triggering on DIS Events

The most reliable signature for the occurrence of a deep inelastic scattering event is the reconstruction of a scattered electron. At the most basic level, the electron is identified as an isolated electromagnetic deposit in the calorimeter. At higher levels of triggering, the calculations for electron identification need not be so fast, so more sophisticated algorithms can be used. An electron can be identified through its shower shape. Electrons emit photons through the process of Bremsstrahlung when they are accelerating or decelerating. The shower that is produced deposits all its energy in the electromagnetic portion of the calorimeter, and has, therefore, a very short longitudinal profile.

7.1.1 GFLT

At the first stage of triggering, global information is taken from the CFLT and the CTD FLT to make loose selections on possible DIS event candidates. Global sums such as total energy in the calorimeter or total transverse energy are used in combination with loose tracking requirements to distinguish classes of real physics events. In order to be included in the event sample used for the measurements described here, one of the following combinations of requirements on the calorimeter energy sums and CTD tracks must have been met. In order for a track in the CTD to be considered a “good track” it must have a z position in the first superlayer between -50 cm. and 80 cm. These requirements are equivalent to a selection of one of the GFLT slots 4074.

- $E^{CAL} > 15GeV$ with a good track
- $E_T^{CAL} > 30GeV$ or $E_T^{CAL} > 11.6GeV$ with a good track
- $E^{EMC} > 15GeV$ or $E^{EMC} > 10GeV$ with a good track
- $E^{BEMC} > 3.4GeV$ with a good track or $E^{BEMC} > 4.8GeV$ with track
- $E^{REMC} > 3.4GeV$ or $E^{REMC} > 2GeV$ with a good track

7.1.2 GSLT

At the second level, information from most detector components is available for triggering, and basic quantities such as $E - p_z$ of the calorimeter energies is used to reject large sources of background. $E - p_z$ is also a useful quantity for selecting DIS events. Events in which the particles emitted from the hard scattering are completely contained in the detector will have an $E - p_z$ of 55 GeV. Since the +z axis is defined to be along the proton beam direction, the $E - p_z$ of the incoming proton is 0, while the $E - p_z$ of the incoming electron is $27.5 - (-27.5) = 55 \text{ GeV}$. By conservation of energy and momentum, the total outgoing $E - p_z$ must also sum to 55 GeV, provided all the outgoing energy is correctly measured. A measurement of the event vertex is made using only the axial wires of the CTD (z-by-timing) [], but with rather poor resolution. Further cuts can be applied to the timing of the calorimeter energies in order to reject beamgas background, sparks and cosmic ray events.

This analysis requires SFEW SLT trigger slot 6 to fire. The requirements of this slot are the following:

- $E^{REMC} > 2.5 \text{ GeV}$ or $E^{BEMC} > 2.5 \text{ GeV}$ or $E^{FHAC} > 10 \text{ GeV}$ or $E^{FEMC} > 10 \text{ GeV}$
- $E - p_z + 2 \text{ Lumi}\gamma > 29 \text{ GeV}$. The lumi gamma measurement is included for ISR events (see Sec. 4.5) in which the emitted photon escapes down the RCAL beampipe. This loss of energy makes the calorimeter measurement of $E - p_z$ alone insufficient.

7.1.3 TLT

Once the second level trigger decision is made, the measurements made by all components of the detector are sent to the event builder for full reconstruction by the TLT.

The third level trigger is made up only of calculations and programs run on detector quantities that were already available at the SLT instance, the full tracking reconstruction is run and jet finding using two different algorithms is performed. Four different electron finders are run in order to select electron candidates as efficiently as possible. [possible detailed explanation of the finders to go here] much improved vertex-finding algorithm is run at the TLT. This improves the $E - p_z$ measurement with respect to the SLT, and a tighter cut $E - p_z + 2 \times \text{Lumi}\gamma > 30 \text{ GeV}$ is applied to further reduce background.

The events for this analysis are selected with the SFEW TLT filters DIS03 or DIS04. DIS03 is the medium Q^2 filter that requires either a Sinistra or Emille electron to be found with at least 4 GeV of energy and outside a radius of 25cm. on the face of the RCAL. For an event vertex at the nominal z=0 position, this radius cut corresponds to a Q^2 cut $Q^2 > 20 \text{ GeV}$. DIS04 is the high- Q^2 trigger that requires one of the four electron finders to find an electron with energy $E_{el} > 7 \text{ GeV}$ outside a boxcut of 30x30 cm.

Once the TLT has made its selection, a further software selection is made which groups events according to DST bits. This analysis requires DST bits 9,11, or 13 to fire. Once this final selection is made, the events are written to tape.

7.2 Offline Event Reconstruction

Once the events are triggered and written to tape, a more precise reconstruction of the event quantities can be performed. The data is also corrected to ensure the fundamental measurements (i.e. cell energies) are accurate and reliable. Before any quantity that relies on the calorimeter measurement is calculated, noisy calorimeter cells are removed by the NOISE96 routine. This noise typically comes from electrostatic discharge between the high voltage bases of the photomultiplier tubes.

An additional correction is made to the cells, using the routine RCALCORR. This routine recalibrates the calorimeter cells so that the energy response in data and Monte Carlo are the same. This correction makes up for deficiencies in the Monte Carlo's ability to reproduce the data, which is necessary for the extraction of any cross section. The calibration factors are determined by two different methods, depending on whether the factor is to be applied to the RCAL or the BCAL cells (no alteration of the FCAL cells is made). For high Q^2 events where the electron is scattered at an angle inside the CTD acceptance region, the calorimeter measurement of the electron energy can be compared to the electron energy calculated using the double-angle method (see Sec.6.1). The double angle method is more reliable because the position resolution of tracks in the CTD is very good, and the difference between the two measurements is taken as the calibration factor. For recalibration in RCAL, kinematic peak events are used. Events are selected with a scattered electron very close to the RCAL beampipe and at low y , in order to select a sample whose distribution of electron energies peak at 27.5, the incoming beam energy. The difference between the observed peak and 27.5 is taken as the calibration factor for RCAL.

A neural network is used to identify the scattered electron, and subdetectors are used to correct the electron's energy and position (see next section). The angle of the hadronic system is corrected using the CorandCut routine. This routine is an iterative algorithm for removing energy deposits that are far from the initial calculation of the hadronic angle and have a timing measurement inconsistent with the ep collision. A jet finder is run on the cell energies included in the hadronic final state. However, both electromagnetic and hadronic deposits in the calorimeter that are well-reconstructed are not necessarily equal in energy to the electron and groups of particles that make up a jet. This is because the particles emitted from the hard scattering must travel a long distance before reaching the calorimeter, and travel through other parts, so-called dead material, of the detector. The particles lose some of their energy while traversing the detector, and this loss in energy needs to be corrected for in the offline event reconstruction.

7.2.1 Positron Reconstruction

Positron candidates are identified using the neural network program Sinistra. This program takes the transverse and longitudinal energy profiles of electromagnetic cells (grouped into islands) from the entire calorimeter as input and calculates the probability (between 0 and 1) that each electromagnetic island resulted from a real scattered electron. The program is trained on neutral current DIS Monte Carlo, and is 80% efficient at finding electrons if the energy of the electromagnetic deposit is larger than 10 GeV and the probability given by

Sinistra is larger than 0.9

Sinistra delivers a list of candidates along with their properties and orders them according to their probability. If 2 or more candidates have the same probability, the one with the highest energy is considered the leading candidate (Findis Option 1). To estimate how much energy the electron lost due to showering in the dead material, the SRTD or RCAL Presampler measurements are used. The electron position is corrected by either the SRTD, HES or by a matching track. This prescription for correcting the electron was developed for the 96/97 F_2 analysis [1].

7.2.2 Jet Reconstruction

The jet finding is performed on all cells associated with the hadronic final state of the event. That is, the cells associated with the most probable Sinistra electron candidate are removed and the jet finder is run on all remaining energy deposits in the calorimeter.

7.2.3 Jet Energy Correction

Correcting for the energy lost by a jet in the dead material of the detector is more complicated than for the electron. Because jets are sprays of various particles, all which interact with matter differently, measuring the energy loss with a pre-shower detector is not possible. Instead, we rely on the Monte Carlo simulation of the dead material. The length of the dead material the jet must pass through is dependent on its polar angle. Therefore, the full pseudorapidity region which is measured is divided into 20 slices, each covering 0.2 units in η . In each region, a profile plot is made of the detector jet's transverse energy in bins of the hadron level jet's transverse energy. A two-line fit of the dependence is made, one with $E_{T,jet}^{HAD} < 40 GeV$, the other with $E_{T,jet}^{HAD} > 40 GeV$ as shown in Figure 13. The parameters of the fit are extracted and applied as corrections to the data.

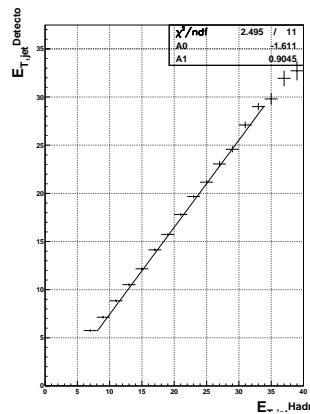







Figure 13: Profile plot of detector level jet transverse energy in bins of hadron level jet transverse energy for NC DIS Monte Carlo. The jet transverse energy in the data is scaled by the parameters of this fit.



7.2.4 Cuts to Reject Background

To further ensure that DIS events are selected and to clean the sample of questionable DIS signatures, the following requirements are made of the data and detector level Monte Carlo.

- $|Z_{vtx}| < 50cm$. A found vertex by the CTD in this range ensures that the event is well contained within the acceptance of the detector and that the angles of the electron and hadronic system are well-reconstructed.
- $38 < E - p_z < 65$ This cut removes photoproduction events and events in which a significant portion of the energy escapes down the RCAL beampipe.
- $y_{el} < 0.95$ There is a small class of events in which a photon or neutral pion fakes the signature of an electron in the forward region of the detector, resulting in very high values of y_{el} . This cut removes those events.
- $p_T^{CAL} / \sqrt{E_T^{CAL}} < 3$. This cut removes cosmic ray events. DIS events should have total transverse momentum $p_T^{CAL} \sim 0$. Most cosmic ray events are cut by the timing requirements at the GSLT, but this requirement removes the small class of cosmic events in which the muon travels through the center of the BCAL at the same time as the beam bunches cross inside the detector and has, therefore, an acceptable timing.
- $|X_{el}| > 14$ || $|Y_{el}| > 14$ where X_{el} and Y_{el} are the raw (uncorrected) positions of the electron on the face of the calorimeter. This “boxcut” removes events in which the electron impacts the detector close to the beampipe where the reconstruction of the electron is ery good.
- $E^{NotInCone} / E_{el} < 0.1$ where $E^{NotInCone}$ is the energy inside a cone of radius 0.8 around the electron not associated with the electron itself. This isolation requirement rejects events in which the electron is not well-separated from the jet and cannot be properly reconstructed.

7.2.5 Phase Space Selection

The phase space selection is made where BFKL dynamics might be ~~present~~ given the acceptance limitations of the detector. To reach a kinematic region where BFKL effects might be visible, it is necessary to measure as low in Q^2 and $E_{T,jet}$ as possible. Because BFKL dynamics are expected to be a small effect and because no NLO BFKL calculation was available at the time of this analysis, we attempt ~~here~~ to look for a breakdown of the NLO QCD prediction using DGLAP evolution. The measurement is initially made as inclusively as possible, where NLO QCD is expected to reproduce the data well. It is then made a second time in a ~~more~~ restrictive phase space in order to select out quark-parton model (QPM) events. is second phase space region will henceforth be referred to as “BGF Phase space.” The measurement is made a third time in the phase space prescribed by Mueller for BFKL searches. is third phase space region will henceforth be referred to as “BFKL Phase Space.”

The jet finding in all three measurements is performed in the laboratory frame. Although jet measurements made in the Breit ne have certain theoretical advantages, they have the major drawback ~~of~~ this measurement of

implicitly selecting at least two high- E_T jets. In order to retain the region of phase space where there are two jets, one with high- E_T and one with low- E_T , the jet finding needs to be performed in the laboratory frame.

Listed below are the common cuts made on data and detector level Monte Carlo for all three measurements. They are exactly the phase space requirements put on the inclusive measurement.

- $Q^2 > 25\text{GeV}^2$ This cut is made to select events above the Q^2 limit imposed by the trigger.
- $y_{jb} > 0.04$. This cut ensures good reconstruction of the hadronic system, which is necessary for the double-angle reconstruction of the kinematics.
- $E_{el} > 10\text{GeV}$ of the Sinistra95 most probable candidate is the region where Sinistra can select positrons with an efficiency greater than 80%.
- $E_{T,jet} > 6\text{GeV}$ and $-1 < \eta_{jet} < 3$. ~~Jet cuts are selected to~~ ensure the jets are well measured. At low transverse energies and high pseudorapidity, the jet finding efficiency and purity is low because either the jets lose a large fraction of their energies in dead material or a portion of their energy escapes down the FCAL beampipe.

For the BGF enhanced measurement, the following additional requirements are made:

- $\cos\gamma_h < 0$. This requirement ensures that the hadronic angle is found in the rear half of the detector. This cut, in combination with the following one, effectively removes QPM events where the jet axis is aligned with the hadronic angle.
- $\eta_{jet} < 0$. This is needed for reliable predictions of the NLO calculation.

For the BFKL measurement, the following additional requirements are made:

- $0.5 < E_{T,jet}^2/Q^2 < 2$. This requirement limits the Q^2 evolution of the particles on the gluon ladder.
- $x_{jet} > 0.036$ where x_{jet} is the fraction of the proton's momentum carried by the jet.

8 Description of the analysis

8.1 Preliminary Studies of Jet Cross Sections in the Breit Frame

8.2 Inclusive Jet Cross Section

8.2.1 Control Plots

8.2.2 Resolutions

8.2.3 Purities, Efficiencies, Correction Factors

8.3 BGF Enhanced Phase Space Cross Section

8.3.1 Control Plots

8.3.2 Resolutions

8.3.3 Purities, Efficiencies, Correction Factors

8.4 Forward Jet Cross Section

8.4.1 Control Plots

8.4.2 Resolutions

8.4.3 Purities, Efficiencies, Correction Factors

9 Results

9.1 Measurement of the inclusive jet cross section

9.2 Measurement of the inclusive jet cross section in the BGF enhanced phase space

9.3 Forward jet cross section

9.4 Systematic Uncertainties

10 Conclusion

References

.

Label	η_{LL}^u	η_{LR}^u	η_{RL}^u	η_{RR}^u	η_{LL}^d	η_{LR}^d	η_{RL}^d	η_{RR}^d
VV	+1	+1	+1	+1	+1	+1	+1	+1
AA	+1	-1	-1	+1	+1	-1	-1	+1
VA	+1	-1	+1	-1	+1	-1	+1	-1
X1	+1	-1	0	0	+1	-1	0	0
X2	+1	0	+1	0	+1	0	+1	0
X3	+1	0	0	+1	+1	0	0	+1
X4	0	+1	+1	0	0	+1	+1	0
X5	0	+1	0	+1	0	+1	0	+1
X6	0	0	+1	-1	0	0	+1	-1
U1	+1	-1	0	0	0	0	0	0
U2	+1	0	+1	0	0	0	0	0
U3	+1	0	0	+1	0	0	0	0
U4	0	+1	+1	0	0	0	0	0
U5	0	+1	0	+1	0	0	0	0
U6	0	0	+1	-1	0	0	0	0

Table 2: The 30 scenarios for a better life considered in this paper. Each row of this table corresponds to two different scenarios for overall interference signs $\epsilon = +1$ and $\epsilon = -1$, respectively.

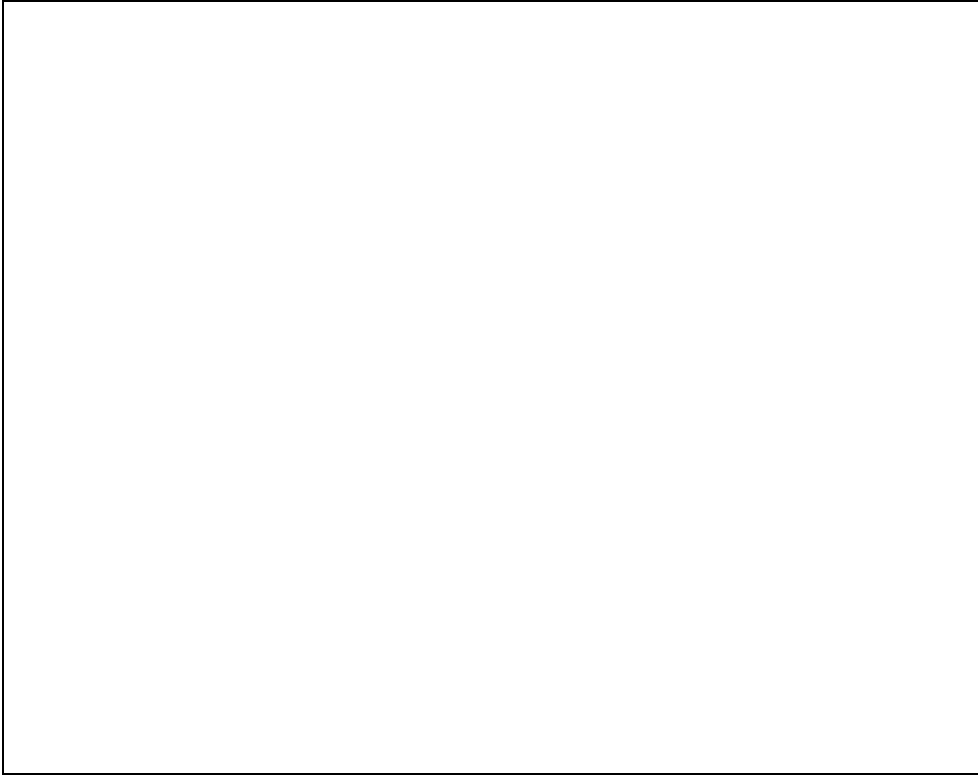


Figure 14: Life beyond the Standard Model.